

# Worldwide Physics-Based Lifetime Prediction of c-Si Modules Due to Solder-Bond Failure

Reza Asadpour , Member, IEEE, Muhammed Tahir Patel , Steven Clark , Nick Bosco ,  
Timothy J. Silverman , and Muhammad A. Alam , Fellow, IEEE

**Abstract**—Lifetime prediction of the fielded c-Si solar modules due to location-specific weather conditions has been an important topic of photovoltaic research and the economic viability of solar energy. Data analytic techniques such as the performance ratio method, Statistical clear sky model, and Suns-Vmp methods quantify the degradation from measured data of a solar farm, however, the nonlinear time-dependence and correlated degradations make it difficult to use the empirical degradation rates for ultimate lifetime projection. In this article, we propose a complementary physics-based model to predict the solder bond failure caused by mechanical stress associated with the variations of the temperature. Integrating the worldwide weather information from NASA/NSRDB databases, the model predicts the location-specific output-power degradation and the lifetime of a module due to solder bond failure. The model parameters are calibrated against qualification tests involving thermal cycling of specific batches of modules from a specific technology/manufacturer. The results may be summarized as: 1) Modules installed at higher latitudes show a longer lifetime due to reduced damage accumulation. 2) The reduction of temperature fluctuation close to large bodies of water, such as seashores, increases solder bond lifetime significantly. 3) Relatively speaking, modules installed close to the Tropic of Cancer/Capricorn (23.5° North/South) suffer from a higher solder bond damage and have a shorter lifetime, suggesting a conservative design. This model should serve as a building block of a comprehensive reliability framework that can predict the lifetime of a module that experiences simultaneous and correlated degradation mechanisms involving yellowing, corrosion, and potential-induced degradation.

**Index Terms**—Characterization, lifetime prediction, output power, predictive modeling, qualification test, series resistance, solder bond failure.

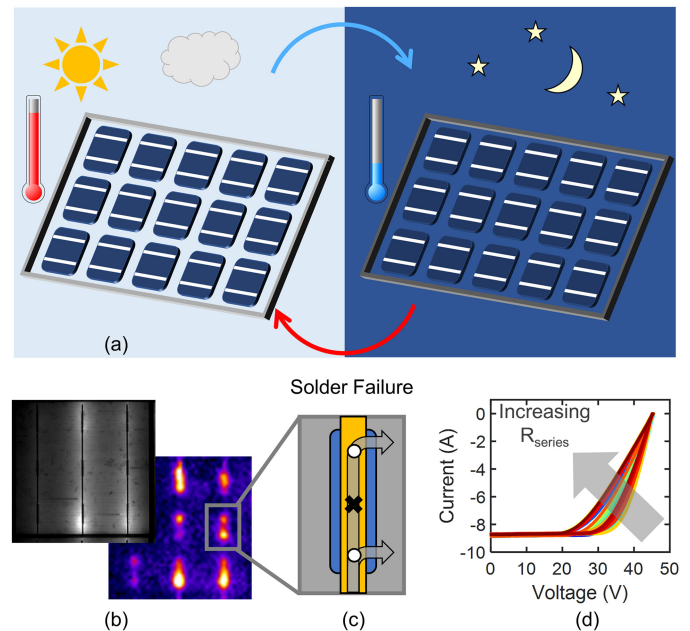


Fig. 1. Thermal cycling results in solder bond failure. (a) Daily temperature variation is the most important cause of accumulated stress that leads to solder bond failure. (b) Electro-luminescence and dark lock-in thermography show certain hotspots in the location of the broken solder pads in the cell. (c) Schematic shows the solder failure causes hotspots and increase in the series resistance. (d)  $I$ - $V$  measurements contain *module-level* series resistance information [14].

## I. INTRODUCTION

THE lifetime of a solar module depends on the local weather conditions, and yet, given the impossibility of testing a new technology for all the climatic conditions across the world, one must instead rely on various conservative accelerated qualification tests to assess the viability of the technology in the field. Although accelerated tests are designed with great care to activate individual degradation mechanisms (e.g., [1]–[5]), it is often not known *a priori* how they translate to actual operating conditions.

For instance, the thermal cycling (TC) test evaluates the reliability of a module subjected to daily and seasonal change of temperature that leads to solder bond failure, finger breaks, accelerated damage in cracked cells, etc. [6]–[12], see Fig. 1(a). The contraction and expansion of different parts of the module that have a mismatched coefficient of thermal expansion result in drastic stress at various interfaces including solder bonds.

Manuscript received July 8, 2021; revised September 6, 2021 and November 12, 2021; accepted December 10, 2021. This work was supported by the National Science Foundation under Grant 1724728 at Purdue University, in part by National Renewable Energy Laboratory, operated by Alliance for Sustainable Energy, LLC, for the U.S. Department of Energy under Grant DE-AC36-08GO28308, and in part by the U.S. Department of Energy Office of Energy Efficiency and Renewable Energy Solar Energy Technologies Office. (Corresponding author: Muhammad A. Alam.)

Reza Asadpour, Muhammed Tahir Patel, and Muhammad A. Alam are with the School of Electrical and Computer Engineering, Purdue University, West Lafayette, IN 47907 USA (e-mail: rasadpou@purdue.edu; patel707@purdue.edu; alam@purdue.edu).

Steven Clark is with the San Diego Supercomputer Center, La Jolla, CA 92093 USA (e-mail: smclark@sdscc.edu).

Nick Bosco and Timothy J. Silverman are with the National Renewable Energy Laboratory, Golden, CO 80401 USA (e-mail: nick.bosco@nrel.gov; timothy.silverman@nrel.gov).

Color versions of one or more figures in this article are available at <https://doi.org/10.1109/JPHOTOV.2021.3136164>.

Digital Object Identifier 10.1109/JPHOTOV.2021.3136164

As a result, the ribbon/busbar interface is likely to fail after an extended period of stress due to weathering, see Fig. 1(b) and (c). Typically, a module consists of a front ribbon made of copper, front solder bonds/pads, silver contacts (fingers and busbars), rear aluminum contacts, rear solder, rear ribbon made of copper, and other intermodule connections as metallic components [11]. The degradation of these interfaces manifests itself as a specific signature on the  $I$ - $V$  characteristics, Fig. 1(d). As discussed in [13] and [14], the solder bond failure causes an increase in the series resistance of the module output characteristics that can be identified and measured by the reduced slope of the  $I$ - $V$  curve close to the  $V_{OC}$  of the module.

There have been many efforts to model the lifetime of a module that is affected solely by solder bond failure. One method of solder joint lifetime modeling, which is not limited to PV modules, starts from calculating accumulated creep energy and strain due to temperature variation cycles. Then, fatigue lifecycles are translated to lifetime. [10], [15]–[18]. The issue with this method is that the life cycle is defined for the controlled temperature condition and not for the ambient temperature. There are other methods that use the finite element method (FEM) to find the fatigue damage accumulated in the solder bonds [10], [11]. However, the model by Jiang *et al.* [10] relies on the average temperature of the module, and therefore, cannot account for the excess stress caused by the cyclic variation of the ambient temperature. Jabarullah *et al.* [11] correlated the fatigue damage to the number of thermal cycles. They use Monte Carlo simulation to find the distributed damage, and then extract the solder bond lifetime, however, it does not provide a compact analytical formulation suitable for location-specific lifetime prediction under actual weather conditions. More importantly, the existing models do not predict the electrical consequences of the mechanical damage.

In this article, we propose a physics-based model that can predict the power loss and lifetime of a c-Si solar module subjected to solder bond failure. We provide the missing link between mechanical and electrical aspects of solder bond failure by using a novel strategy to extract key parameters of the model by reinterpreting the TC data. We will see that the rate of solder bond failure is related to environmental factors such as ambient temperature, incident light, etc. In addition, we will use a mathematical technique to account for the statistical distribution of the failure time distribution of individual solder bonds. This powerful model uses location-specific ambient conditions; therefore, it can predict the accumulated degradation of a module installed worldwide. This article is an extended version of our article, presented at the 2021 IEEE Photovoltaic Specialists Conference [19]. The rest of this article is organized as follows. In Section II, we explain the simulation framework by calibrating the experimental results of a TC test for specific models of manufacturers of c-Si modules discussed in [8] against the accumulated damage found based on the work of Bosco *et al.* [20] using the Markov chain method. Bosco *et al.* [20] take into account ambient temperature and the material properties of the solder bonds while the Markov method includes the statistical nature of the solder bond failure bridging the mechanical damage ramifications to the electrical outcome. Then, in Section III,

we use the developed model to find the lifetime of modules installed at different locations worldwide and see how the latitude, longitude, and specific geographical features dictate in the predicted lifetime. We emphasize that the lifetimes predicted are based on similarly processed batches of modules with a specific technology/manufacturer reported in [8]. Indeed, the lifetime would increase considerably for a technology with improved process control. Finally, Section IV concludes this article.

## II. THEORY AND SIMULATION FRAMEWORK

There are three components of the phenomenological model of the location-specific time-dependent series resistance increase due to solder bond failure: 1) inelastic strain energy density or damage accumulation due to temperature cycling, ( $D(x, y, t)$ ); 2) probability of breaking of the solder bond once critical damage has been accumulated, ( $P_n(x, y, t)$ ); and 3) the effect of the broken solder bonds on the  $I$ - $V$  characteristics of the solar module, ( $R_s(x, y, t)$ ). For the first step, we will use the work of [20] to find the accumulated damage as a function of temperature variation, as shown in Fig. 3. For the second step, we will explain in Fig. 4 how the sequence of bond breakage occurs as a function of time using the Markov chain method. Although we have focused on discrete solder bonds, the Markov approach is easily adapted to continuously formed layers (such as front solder layers) as well by discretizing the layers into several fictitious segments (in a manner analogous to finite-element modeling). For the third and final step, we will put the degraded cells together to see the electrical consequence of accumulated damage and calibrate the constructed module against TC test results, see Fig. 6. Information in Figs. 5 and 6 would allow us to translate the accumulated damage plotted in Fig. 3 to the solder bond limited lifetime of solar modules shown in Fig. 7.

### A. Accumulated Stress Due to Temperature Variation

Asadpour *et al.* [19] used a detailed physics-based finite-element method to carefully calculate and calibrate the damage accumulated in a solder bond due to location-specific weather conditions. Equation (1) of [20] relates the temperature variation to the accumulated damage, as follows:

$$D(x, y, t) = C(\Delta T)^n (r(T))^b \exp\left(-\frac{Q}{k_B T_{\max}}\right) \quad (1)$$

where  $x$  and  $y$  are the longitude and latitude of a location,  $D$  is the location-specific accumulated damage in kPa,  $\Delta T(x, y)$  is the average of the daily temperature change between the minimum and maximum,  $r(T)(x, y)$  is the number of times that the module temperature is crossing the critical temperature  $T = 55.8$  °C for 30-min interval weather data,  $T_{\max}(x, y)$  is the average of the daily maximum temperature in the course of a year,  $C = 344.1$  is a fitting parameter for 30-min interval weather data (that is essentially identical for 15-min interval data used in this article),  $k_B$  is the Boltzmann constant,  $Q = 0.12$  eV is the activation energy,  $n = 1.9$  and  $b = 0.33$  are power-law exponents for the Coffin–Manson equation. In general, the parameters ( $Q$ ,  $n$ , and  $b$ ) depend on the solder bond eutectic material. Bosco *et al.* [20] used the scaling constant  $C$  (344.1) and the critical temperature

Pursuant to the DOE Public Access Plan, this document represents the authors' peer-reviewed, accepted manuscript.

The published version of the article is available from the relevant publisher.

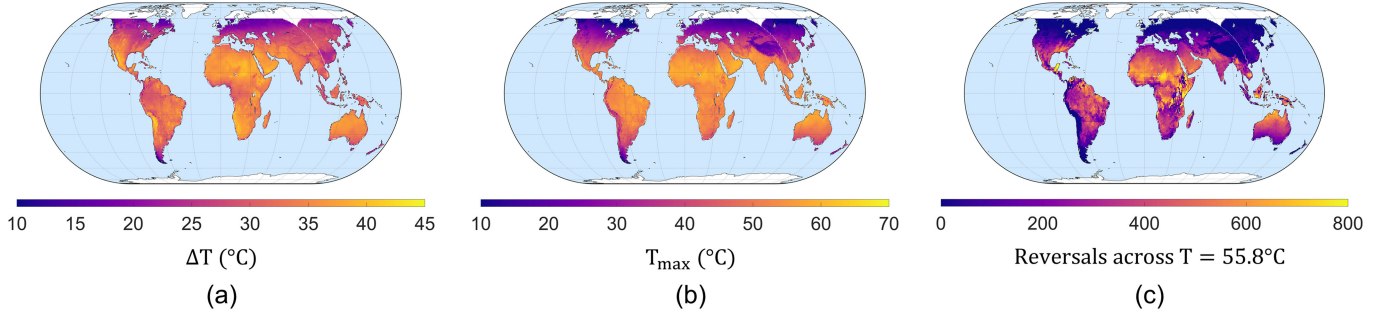


Fig. 2. Global maps of one year data showing (a) the average of the daily temperature change between minimum and maximum ( $\Delta T$ ) of a module (b) average of the daily maximum temperature ( $T_{\max}$ ) of a module and (c) the number of times that the module temperature crosses the critical temperature  $T=55.8$  °C.

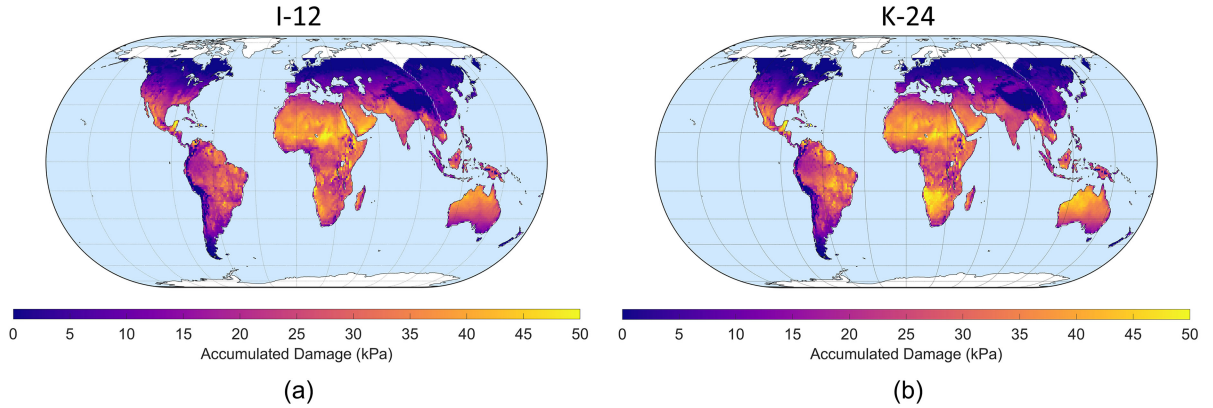


Fig. 3. Accumulated damage calculated based on the data shown in Fig. 2 using (1) over course of one year for modules (a) I-12 and (b) K-24.

$T$  in  $r(T)$  to fit (1) to the accumulated damage results of their FEM simulation at the end of one year of weather data. Therefore, the parameters  $C$  and  $T$  are technology and material-dependent. They also depend on the temporal resolution of the weather data. We use the location weather information plotted in Fig. 2 to determine the accumulated damage of each year separately and add them to find the total accumulated damage. The results are plotted in Fig. 3.

### B. Markov Chain Method Connects Mechanical Stress Damage to the Probability of Solder Bond Failure

The accumulated damage  $D(x, y, t)$  leads to stochastic failure of solder bonds. We use a well-known mathematical technique called the Markov chain model as in (2) [21] to account for the statistical nature of successive solder bond failures, namely

$$P_n(\chi(D), \xi) = \left[ \prod_{m=0}^{n-1} (1 + m\xi) \right] \left( \frac{1 - e^{-(\xi\chi)}}{\xi\chi} \right)^n \frac{\chi^n e^{-\chi}}{n!} \quad (2)$$

where  $P_n$  is the probability of having a cell with  $n$  number of broken bonds and naturally  $\sum_n P_n = 1$ ,  $\xi$  is the correlation factor between the number of broken bonds (higher  $\xi$  implies accelerated solder bond failure due to correlation after the breakage of the first solder bond; in contrast, with  $\xi \rightarrow 0$ , (2) reduces to Poisson failure distribution, as expected),  $\chi = (t/\eta(D(x, y, t)))^\beta$  is the normalized time of TC test or simulation,  $\eta(D(x, y, t))$

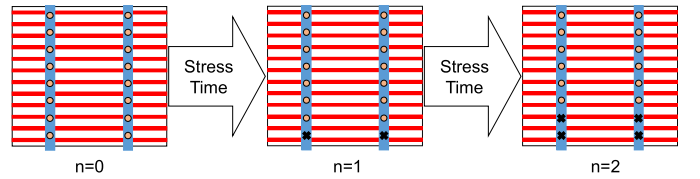


Fig. 4. Top view of a schematic of a c-Si solar cell with two busbars shows sequence of solder bonds being broken. For simplicity, it is assumed that longer stress duration breaks successive rows of solder bonds (black crosses) close to the extraction point.

is the normalization factor and the mean time of first bond failure to occur that is obtained from experimental calibration (see below), and  $\beta \sim 1$  describes the linear increase in failure rate with accumulated damage. A continuum method is justified because there are more than 1200 solder bonds in each module. The Markov chain approach ensures that the sum of the number of healthy and broken bonds remains constant and increase in the number of broken bonds is consecutive (see Fig. 4). For simplicity, we assumed all the bonds that are in the same row will break together, i.e.,  $P_1$  means the probability of having two broken bonds that are in the first row of a single solar cell. Again, given the large number of solder bonds, this approximation cannot affect the results significantly. In addition, we assume the worst-case scenario, i.e., all the bonds break consecutively starting from the bonds closer to the extraction point, as shown in Fig. 4.

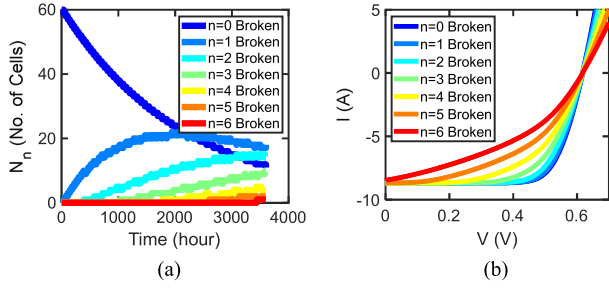


Fig. 5. (a) Calculated number of cells that have different number of rows of broken solder bonds as a function of thermal cycling exposure time. At the beginning, none of the solder bonds of the 60 pristine cells is broken. (b)  $I$ - $V$  curve of simulated cells with different number of rows of broken solder bonds for cells of module K-24.

### C. Constructing $I$ - $V$ of a Module Using Markov Chain Method and $I$ - $V$ of Individual Cells Suffering From Solder Failure

Once we know the probability of cells having zero to six rows of broken solder bonds ( $P_0, P_1, P_2, \dots, P_6$ ), we know the number of cells having a different number of rows of broken solder bonds ( $N_n \equiv N \cdot P_n(\chi, \xi)$ ) at any point in time (see Fig. 5(a)). By putting the Griddler-simulated  $I$ - $V$  curves of the cells [13] with the calculated number of rows of broken solder bonds in series, we can reconstruct the  $I$ - $V$  of the module at hand using

$$V_{\text{module}}(I)(t, x, y) = \sum_{n=0}^{n_{\text{max}}} N_n V_n(I) \quad (3)$$

where  $N_n$  is the number of cells with  $n$  number of broken bonds,  $V_n(I)$  is the corresponding voltage of a cell with  $n$  number of broken bonds, and  $n_{\text{max}}$  is the maximum number of rows of bonds that can be broken, which is 6 in this case. The simulated  $I$ - $V$ s that are generated using the solar cell simulator Griddler [22] are shown in Fig. 5(b).

### D. Calibration Against TC Measurements Determines the Key Parameter $\eta(D)$ for (2)

To calibrate the module technology-specific  $\eta(D(x, y, t))$  in (2), first, we need to run the TC test on a module for a few hundred cycles and measure the  $I$ - $V$  curve every hundred cycles. (Here, we used the data of a module named I-12 and K-24 from [8]). The measured modules have 60 cells, each cell has two busbars, and (we assumed that) each busbar has eight solder bonds. The modules were exposed to a conventional thermal cycling test based on International Standards Protocol (IEC 61215: 2005, Clause 10.11) [23]. Then using Griddler, we match the  $I$ - $V$  of the pristine module with the simulation by putting identical 60 cells in series (see Table I). Obviously, the number of cells depends on the module technology. Next, we match the  $I$ - $V$  at different measured cycles, i.e., 100, 200, 300, and up to 600 cycles. To do so we use (2), (3), and the values of  $\xi$  and  $\eta$  to predict the  $I$ - $V$  characteristics and the normalized output power, as shown in Fig. 6, and adjust  $\eta(D)$  so that the simulated  $I$ - $V$  matches with the measured experiments. In [8], the total stress time is 600 cycles or 3600 h, i.e., six hours for each thermal cycle. The values

TABLE I  
BASELINE SIMULATION PARAMETERS FOR I-12 AND K-24 CELLS IN GRIDDLER

Property (Unit)	Value (I-12)	Value (K-24)
Finger sheet resistance (m $\Omega$ /sq)	3.5	3.5
Busbar sheet resistance (m $\Omega$ /sq)	3	3
Finger contact resistance (m $\Omega$ /sq)	5	5
Layer sheet resistance ( $\Omega$ /sq)	80	65
Wafer internal series resistance (m $\Omega$ .cm <sup>2</sup> )	5	5
Internal shunt conductance (1/( $\Omega$ .cm <sup>2</sup> ))	0	0
Ribbon width (mm)	1	1
Ribbon sheet resistance (m $\Omega$ /sq)	0.1	0.1
Contact point resistance (m $\Omega$ )	0	0
Number of tabbing points on ribbon	8	8
1-sun $J_{ph}$ , non-shaded area (mA/cm <sup>2</sup> )	36.76	37.55
$J_{01}$ , passivated area (fA/cm <sup>2</sup> )	1020	1220
$J_{01}$ , metal contact (fA/cm <sup>2</sup> )	600	760
$J_{02}$ , passivated area (nA/cm <sup>2</sup> )	7	8.7
$J_{02}$ , metal contact (nA/cm <sup>2</sup> )	50	65
Finger pitch (mm)	1.9	1.9
Finger width ( $\mu$ m)	60	60
Number of fingers	82	82
Busbar width (mm)	1.5	1.5
Number of busbars	2	2
Cell area (cm <sup>2</sup> )	243.36	243.36
Front illumination (Suns)	1	1

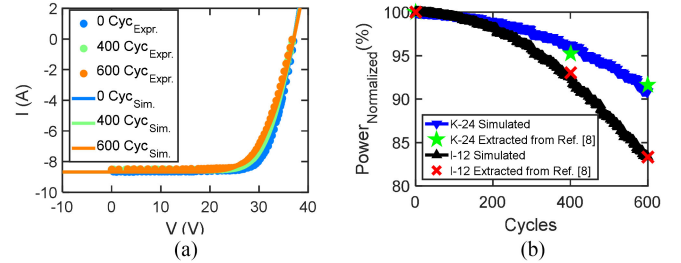


Fig. 6. (a) Module  $I$ - $V$  curve characteristics of experimental and simulated results for module K-24, a properly processed module. (b) Normalized output power of the modules (I-12 and K-24) show good agreement between simulation and experiment verifying that the assumptions were reasonable.

found for the Markov method are  $\xi = 0.1$  and  $\eta = 1500$  h for module I-12 and  $\xi = 0.1$  and  $\eta = 2120$  h for module K-24. Once  $\eta$  is calibrated, we determine the accumulated damage due to TC test that we call critical accumulated damage that is 353 kPa and 405 kPa for our showcase modules I-12 and K-24, respectively. The weather data that causes the same amount of critical accumulated damage determines the new  $\eta$  for any specific location in the world. To find the location-specific  $\eta(D(x, y, t))$  we use (1), however,  $\xi$  remains constant because it only depends on the module technology. Markov chain method dictates that no matter the lifetime value, the normalized lifetime for this simulated module is always  $\chi = t/\eta = 2.675$ . Then, for any location lifetime equals  $2.675 \times \eta(D(x, y, t))$  for our prototype modules. Note that  $\eta(D(x, y, t))$  is a technology-specific parameter that depends on the specific eutectics used, number of bond-pads, the module dimensions, module framing, and manufacturing process. Hence, the lifetime results and  $\eta(D(x, y, t))$  presented in this article are derived specifically for I-12 and K-24 modules reported in [8]. The lifetime of the I-12 module can enhance

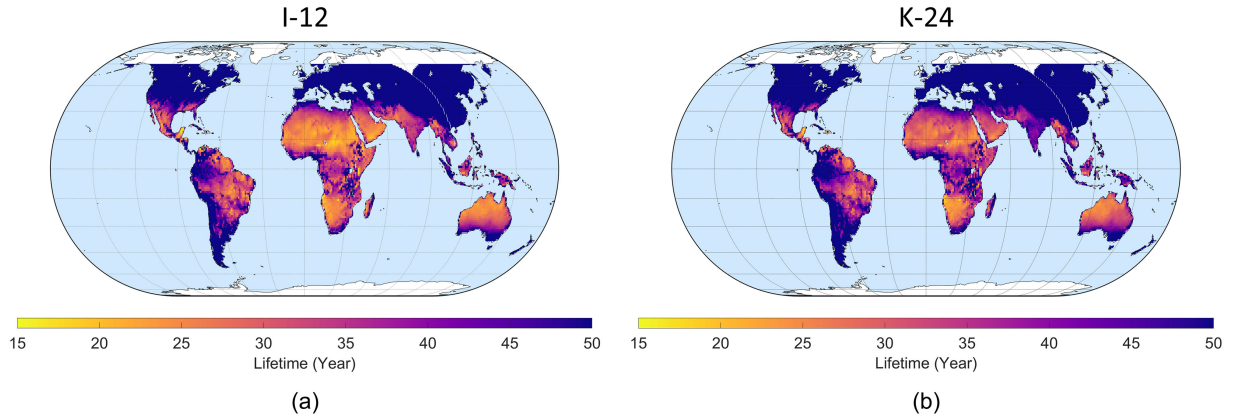


Fig. 7. Predicted lifetime of modules (a) I-12 and (b) K-24 installed at different locations worldwide. Lifetime of 50 years and more are shown as dark violet.

significantly with improved solder-bond processing and process control as discussed in [8], however, the K-24 module does not show manufacturing issues. The general approach presented here can be used to see if specific batches of similarly processed modules from a given technology/manufacture have sufficiently reliable solder bonds for a specific location based on the parameters derived from the qualification tests. Therefore, one must conduct cycle-dependent TC experiments for each new technology/manufacture before its worldwide failure probability and lifetime are calculated.

As an aside, we use Griddler to determine the 2-D distributed electron/hole collection to eventually calculate the  $I$ - $V$  characteristics of a solar cell. Thus, our model can equivalently analyze the effects of discrete solder-pad breakage or partial breakage of a continuous solder-layer on equal footing. Furthermore, the experiment in [8] measures the  $I$ - $V$  at the module level and not the cell level. The 60 cells per module, two busbars per cell, and eight pads per busbar mean that there are approximately 1000 pads per module. Statistically, the sequential discrete failure of this large number of bonds (pads) would be indistinguishable compared to the gradual failure of continuous solder bonds. This justifies the comparison of simulated results based on a discrete failure of solder bonds versus experimentally measured results of a solar module with a continuous solder layer. Fig. 6 shows a good agreement between simulation and measured values verifying our assumptions.

### III. RESULTS AND DISCUSSION

To illustrate the methodology, we downloaded the weather data from the NSRDB NASA database [24]. We used PSM v3 5-min subdatabase for the Continental United States (two years of data), MSG IODC: PSM v3 for Africa and parts of Europe and Asia (three years of data) with a 15-min temporal resolution, PSM v3 for the above Continental United States up to 60-degree latitude and northern parts of South America (two years of data), Full Disc for southern parts of South America (one year of data), and Himawari for Australia and eastern parts of Asia (four years of data) that have a 30-min temporal resolution.

We use King's model as described in (4) [25] to find the cell temperature using ambient temperature ( $T_{amb}$ ), global irradiance ( $E$ ), and wind speed (WS).

$$T_{cell} = T_{amb} + E \cdot \exp(a + b \cdot WS) + E \frac{\Delta T}{E_0} \quad (4)$$

where  $a = -3.56$  and  $b = -0.750$  are empirically determined coefficients for open rack glass/cell/polymer/backsheet module structure,  $\Delta T$  is the temperature difference between the cell and module back surface and it is determined to be 3 °C for this configuration, and  $E_0$  is the reference solar irradiance on the module with the value of 1000 W/m<sup>2</sup>. Here, we use global horizontal irradiance for the local irradiance intensity ( $E$ ), so that we can account for reduced self-heating when a fraction of the plane-of-array incident power is converted to electricity.

Utilizing all the calibration and weather data, the world map of the predicted lifetime in Fig. 7 is simulated. This map provides three key observations: 1) Modules that are installed at higher latitudes show a longer lifetime as they accumulate less damage to cause solder bond failure. This can be explained based on Fig. 2(a)–(c), since  $T_{max}$  is much lower than the critical temperature and  $\Delta T$  is lower compared to lower latitudes, the number of reversals is considerably lower than the other locations causing less damage to be accumulated and hence longer lifetime is predicted. 2) Closer to a large body of water and in the coastlines, the solder bond lifetime can be longer. Due to higher relative humidity close to the coastlines the temperature variation range decreases, as can be seen in Fig. 2(a), and the number of reversals drops in these regions (see Fig. 2(c)) and as a result the damage reduces, and lifetime increases. 3) Regions adjacent to/within the Tropic of Cancer and Capricorn (23.5° North and South) are the regions with a shorter solder bond lifetime. These regions have higher  $T_{max}$  and their location with a dry and hot climate makes the  $\Delta T$  and daily temperature variation higher. Therefore, the number of reversals increases causing the accumulated damage to rise and the lifetime to be shortened (see Fig. 2(a)–(c) and Fig. 3). The equator shows a moderate lifetime compared to the Tropic of Cancer and Capricorn due to their lower  $T_{max}$ , which is partially the result of incident sunlight not being normal at these locations.

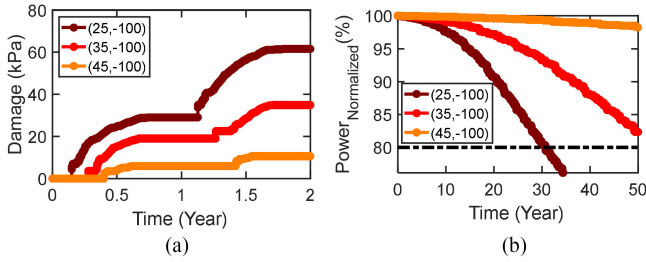


Fig. 8. (a) Normalized output power and (b) accumulated damage of a module at longitude  $-100^\circ$  and different latitudes ( $25^\circ$ ,  $35^\circ$ ,  $45^\circ$ ). The dashed line marks the lifetime when the normalized power reaches 80% of its initial value.

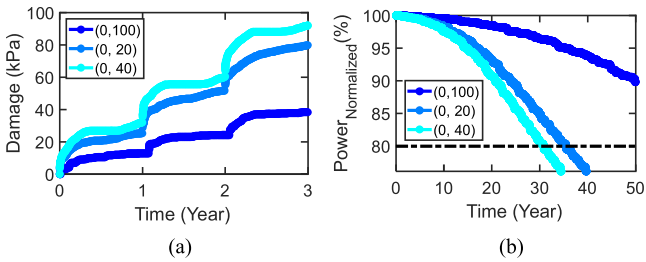


Fig. 9. (a) Normalized output power and (b) accumulated damage of a module at equator  $0^\circ$  and different longitudes ( $20^\circ$ ,  $40^\circ$ ,  $100^\circ$ ). The dashed line marks the lifetime when the normalized power reaches 80% of its initial value.

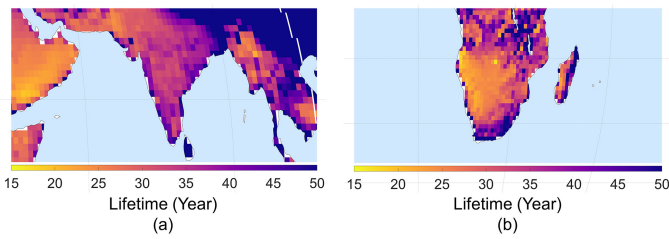


Fig. 10. Zoomed-in map of (a) Indian subcontinent and (b) the Cape of Good Hope as two examples of increased lifetime close to large bodies of water due to lower temperature fluctuations.

Fig. 8 shows the general impact of varying latitude on output power, lifetime, and accumulated damage. Locations above Tropic of Cancer with lower latitude are generally warmer: the increase in  $T_{\max}$  and the number of crossings  $r(T)$  reduce the lifetime.

Although the longitude is not expected to have a significant effect on the lifetime, we see that lifetime increases when the location is closer to the seashore or oceans, as shown in Fig. 9. For instance, as shown in Fig. 9 (0,100) is a location in Indonesia that is close to the Pacific Ocean. Fig. 10 illustrates a zoomed-in map of the Indian subcontinent and the Cape of Good Hope as two regions with longer lifetimes close to the seashores.

The general results and the trend of the lifetime in different world regions are relatively correct, but in a specific location, more accurate local data are necessary for an exact lifetime prediction. Furthermore, the absolute lifetime depends on the model used for calculating the panel temperature. We have calibrated our model for similarly processed batches of a specific

manufacturer in this article and the results need to be interpreted accordingly. The methodology developed, however, is versatile and can be used for calibration and world-wide prediction of solder bond lifetime of any technology.

#### IV. CONCLUSION

The temporal resolution of the weather data plays an important role in the accuracy of the predicted lifetime. With higher temporal resolution, the number of reversals across the critical temperature  $r(T)$  increases, but some of the reversals may be too short to contribute to accumulated damage. In this article, we used 15-min and 30-min resolution data provided by NSRDB data viewer and made sure that the resulting accumulated damage without exponentially weighted moving average (EWMA) matches reasonably well ( $\pm 20\%$ ) with the values reported by Bosco *et al.* [20] that used 1-min temporal resolution. However, if one wants to use higher resolution then it is advised to adapt the EWMA which is described in [20].

In this article, we have also emphasized the importance of calibration measurement during the TC test. We have discussed the calibration process in detail in Section II and, we have emphasized the need for a set of *full I-V* characteristics of the modules collected by periodically interrupting the TC test. Without these measurements at different stages of the TC test, it is impossible to track, based on the changes in the series resistance, the average number of broken bonds of the module undergoing the TC test.

To summarize, we have proposed a physics-based model that predicts the lifetime of a module that suffers only from solder bond failure due to temperature variation. Our Markov chain-based model combines, for the first time, mechanical and electrical aspects of solder bond failure and directly correlates location-specific thermal cycling to the efficiency degradation of a solar module and allows us to quantify the dramatic variation of the location-specific lifetime across the world and deduce three main conclusions.

- 1) The modules that are installed at higher latitudes accumulate less damage and have longer lifetime.
- 2) Close to a large body of water and in the coastlines, solder bond lifetime can be longer.
- 3) Adjacent to or within the Tropic of Cancer and Capricorn ( $23.5^\circ$  North and South) installed modules are more likely to suffer from higher solder bond accumulated damage and have a shorter lifetime.

Coupled with other degradation modes, the approach proposed in this article defines the first step towards a predictive reliability model that uses the results of the qualification test for location-specific lifetime prediction across the world.

The major point of this article is that the proposed physics-based model links the results of a qualification test to satellite-derived weather information to the mechanical damage model of Bosco *et al.* [20] and then bridges them to the electrical signatures of solder bond failure [13], [14] to reach several important/intuitive conclusions regarding location-specific degradation of a solar module. This article, therefore, would encourage the PV researchers worldwide, such

as India Survey or floating solar groups [26], [27] to rethink reliability issues in a geography-specific context and categorize the failure mechanism of the field degraded modules in terms of their electrical characteristics.

#### ACKNOWLEDGMENT

The authors would like to thank A. C. Catlin and C. P. Hewa Nadungodage from DEEDS at Purdue University for providing us with the platform to store and use the downloaded data from the NSRDB database, and also like to thank Dr. M. Gupta, G. Buster, and P. Edwards from NREL for resolving an issue with data referencing in the NSRDB database. The views expressed in the article do not necessarily represent the views of the DOE or the U.S. Government. The U.S. Government retains and the publisher, by accepting the article for publication, acknowledges that the U.S. Government retains a nonexclusive, paid-up, irrevocable, worldwide license to publish, or reproduce the published form of this article, or allow others to do so, for U.S. Government purposes.

#### REFERENCES

- [1] H. Xiong *et al.*, "Corrosion behavior of crystalline silicon solar cells," *Microelectron. Rel.*, vol. 70, pp. 49–58, Oct. 2017.
- [2] J. Zhu *et al.*, "Changes of solar cell parameters during damp-heat exposure," *Prog. Photovolt., Res. Appl.*, vol. 24, no. 10, pp. 1346–1358, Sep. 2016.
- [3] S. Suzuki, T. Tanahashi, T. Doi, and A. Masuda, "Acceleration of degradation by highly accelerated stress test and air-included highly accelerated stress test in crystalline silicon photovoltaic modules," *Jpn. J. Appl. Phys.*, vol. 55, no. 2, Feb. 2016, Art. no. 022302.
- [4] T. H. Kim, N. C. Park, and D. H. Kim, "The effect of moisture on the degradation mechanism of multi-crystalline silicon photovoltaic module," *Microelectron. Rel.*, vol. 53, no. 9–11, pp. 1823–1827, 2013.
- [5] M. Koehl, S. Hoffmann, and S. Wiesmeier, "Evaluation of damp-heat testing of photovoltaic modules," *Prog. Photovolt., Res. Appl.*, vol. 25, no. 2, pp. 175–183, Feb. 2017.
- [6] Y. J. Jeon, D. S. Kim, and Y. E. Shin, "Study of characteristics of solar cells through thermal shock and high-temperature and high-humidity testing," *Int. J. Precis. Eng. Manuf.*, vol. 15, no. 2, pp. 355–360, Feb. 2014.
- [7] M.-S. Kang, Y.-J. Jeon, D.-S. Kim, and Y.-E. Shin, "Comparison of the 60Sn40Pb and 62Sn2Ag36Pb solders for a PV ribbon joint in photovoltaic modules using the thermal shock test," *Energies*, vol. 10, no. 4, pp. 529, Apr. 2017.
- [8] S. Kawai *et al.*, "Causes of degradation identified by the extended thermal cycling test on commercially available crystalline silicon photovoltaic modules," *IEEE J. Photovolt.*, vol. 7, no. 6, pp. 1511–1518, Nov. 2017.
- [9] Y. J. Jeon, M. S. Kang, and Y. E. Shin, "Growth of an Ag3Sn intermetallic compound layer within photovoltaic module ribbon solder joints," *Int. J. Precis. Eng. Manuf. - Green Technol.*, vol. 7, no. 1, pp. 89–96, Jan. 2020.
- [10] N. Jiang, A. G. Ebadi, K. H. Kishore, Q. A. Yousif, and M. Salmani, "Thermomechanical reliability assessment of solder joints in a photovoltaic module operated in a hot climate," *IEEE Trans. Compon., Packag. Manuf. Technol.*, vol. 10, no. 1, pp. 160–167, Jan. 2020.
- [11] N. H. Jabarullah, A. Surendar, M. Arun, A. F. Siddiqi, and T. Krasnopevtseva, "Microstructural characterization and unified reliability assessment of aged solder joints in a PV module," *IEEE Trans. Compon., Packag. Manuf. Technol.*, vol. 10, no. 6, pp. 1028–1034, Jun. 2020.
- [12] E. H. Amalu, D. J. Hughes, F. Nabhani, and J. Winter, "Thermomechanical degradation of crystalline silicon photovoltaic (c-Si PV) module in operation," *Eng. Failure Anal.*, vol. 84, pp. 229–246, Feb. 2018.
- [13] R. Asadpour, X. Sun, and M. A. Alam, "Electrical signatures of corrosion and solder bond failure in c-Si solar cells and modules," *IEEE J. Photovolt.*, vol. 9, no. 3, pp. 759–767, May 2019.
- [14] R. Asadpour, D. B. Sulas-Kern, S. Johnston, J. Meydbray, and M. A. Alam, "Dark Lock-in thermography identifies solder bond failure as the root cause of series resistance increase in fielded solar modules," *IEEE J. Photovolt.*, vol. 10, no. 5, pp. 1409–1416, Sep. 2020.
- [15] O. O. Ogbomo, E. H. Amalu, N. N. Ekere, and P. O. Olagbegi, "Effect of operating temperature on degradation of solder joints in crystalline silicon photovoltaic modules for improved reliability in hot climates," *Sol. Energy*, vol. 170, pp. 682–693, 2018.
- [16] J. Zhao, Y. Mutoh, Y. Miyashita, and S. L. Mannan, "Fatigue crack-growth behavior of sn-ag-cu and sn-ag-cu-bi lead-free solders," *J. Electron. Mater.*, vol. 31, no. 8, pp. 879–886, 2002.
- [17] J. Mi, Y. F. Li, Y. J. Yang, W. Peng, and H. Z. Huang, "Thermal cycling life prediction of sn-3.0ag-0.5cu solder joint using type-i censored data," *Sci. World J.*, vol. 2014, 2014, Art. no. 807693.
- [18] A. Syed, "Accumulated creep strain and energy density based thermal fatigue life prediction models for snagcu solder joints," in *Proc. - Electron. Compon. Technol. Conf.*, 2004, pp. 737–746.
- [19] R. Asadpour, M. T. Patel, S. Clark, and M. A. Alam, "Worldwide physics-based analysis of solder bond failure in c-Si modules for lifetime prediction," in *Proc. Conf. Rec. IEEE Photovolt. Spec. Conf.*, Jun. 2021, pp. 260–263.
- [20] N. Bosco, T. J. Silverman, and S. Kurtz, "Climate specific thermomechanical fatigue of flat plate photovoltaic module solder joints," *Microelectron. Rel.*, vol. 62, pp. 124–129, Jul. 2016.
- [21] M. A. Alam and R. K. Smith, "A phenomenological theory of correlated multiple soft-breakdown events in ultra-thin gate dielectrics," in *Proc. IEEE Int. Rel. Phys. Symp.*, 2003, pp. 406–411.
- [22] J. Wong, "Griddler: Intelligent computer aided design of complex solar cell metallization patterns," in *Proc. Conf. Rec. IEEE Photovolt. Specialists Conf.*, 2013, pp. 933–938.
- [23] *Crystalline Silicon Terrestrial Photovoltaic (PV) Modules - Design Qualification and Type Approval*, IEC 61215:2005, 2005.
- [24] NSRDB Data Viewer. Accessed: May 5, 2021. [Online]. Available: <https://maps.nrel.gov/nsrdb-viewer/>
- [25] J. A. Kratochvil, W. E. Boyson, and D. L. King, "Photovoltaic array performance model," Sandia Nat. Lab., Albuquerque, NM, USA, Tech Rep. SAND2004-3535, Aug. 2004.
- [26] M. Kumar and A. Kumar, "Experimental characterization of the performance of different photovoltaic technologies on water bodies," *Prog. Photovolt., Res. Appl.*, vol. 28, no. 1, pp. 25–48, Jan. 2020.
- [27] R. Dubey *et al.*, "Comprehensive study of performance degradation of field-mounted photovoltaic modules in India," *Energy Sci. Eng.*, vol. 5, no. 1, pp. 51–64, Feb. 2017.